

Cite this: *Nanoscale*, 2012, **4**, 7149

www.rsc.org/nanoscale

PAPER

Controlling surface plasmon interference in branched silver nanowire structures

Hong Wei^a and Hongxing Xu^{*ab}

Received 20th June 2012, Accepted 8th September 2012

DOI: 10.1039/c2nr31551c

Using quantum dot fluorescence imaging, we investigated the interference of surface plasmon beams in branched silver nanowire structures. Depending on the phases and polarizations of the incident light, interferences of plasmon beams modulate the plasmon propagation in the branched structures and the output light intensity in the distal ends. The interference visibility is strongly dependent on the incident polarization at the main wire terminal, and the mechanism is revealed by quantum dot fluorescence imaging of the near field distribution of propagating plasmons. The near field distribution pattern resulting from the beating of different plasmon modes plays a critical role in the plasmon interference. The overlap of the antinode in the near field pattern with the connection junction in the nanowire structure is required for a large interference visibility, since the overlap makes the electric field intensity difference of the two plasmon beams smaller. It is found that the plasmon interference is strongly dependent on the polarization of the excitation light at the main wire terminal, but weakly dependent on the polarization at the branch wire terminal.

Introduction

The surface plasmon (SP) resonances in metal nanostructures present various optical properties,^{1–3} and have been applied in many different fields.^{4,5} The huge enhanced electromagnetic (EM) field in the junctions of coupled nanostructures can largely enhance the Raman scattering of molecules located at the junctions, so-called “hot spots”,^{6–13} which can even make the detection of single molecules using Raman spectroscopy possible.^{6–8} The EM field enhancement at “hot spots” can also enhance optical force for trapping micro-/nano-structures or molecules.^{14–19} The large enhancement of the EM field has been recently applied to amplify some nonlinear processes.^{20,21} Another optical property of surface plasmon resonances, the frequencies are strongly dependent on the surrounding dielectric environments, has been used for bio or chemical sensing.^{22–24} In recent years, the SP propagation in one dimensional nanostructures has attracted much attention because it could provide a promising avenue towards the optical interconnects between semiconductor electronic devices and plasmonic circuits for future optical computing.²⁵ A few different structures have been investigated as plasmonic waveguide, such as nanoparticle chain,²⁶ metal strips²⁷ and grooves in metal films.^{28,29} To compensate the loss during SP propagation, signal magnification by gain media was demonstrated.³⁰ Intensive theoretical studies

have been performed, such as the interaction of narrow-spaced nanowires,³¹ the coupling efficiency of plasmons and photons,³² the propagating plasmonic wave packets in metal nanowires,³³ and combined surface plasmon and classical waveguiding through metamaterial fiber design.³⁴

As very simple and proof-of-principle plasmonic waveguides, chemically synthesized silver nanowires (NWs) are attractive for both fundamental researches and demonstration of potential applications due to their crystalline structures which result in the low energy loss for propagating plasmons in optical frequencies. Many interesting studies on chemically synthesized NWs have been performed recently. It has been demonstrated that the Ag NWs can function as efficient SP Fabry–Perot resonators,³⁵ and the SPs are scattered out as photons at the output terminal of the NW and emit in a certain direction with polarizations depending on the geometries of the NW.^{36–38} The group velocity of plasmons propagating in Ag nanowires can be measured by spectral interferometry.^{39,40} The SPs can be excited or coupled out by the coupling between Ag NWs and emitters,^{41–47} and coupled from/into the light propagating in semiconductor NWs.^{48,49} The propagating plasmons have also been employed to remotely excite the Raman scattering even at the single molecule level.⁵⁰ Energy loss induced by the proximal substrate and the bending of the Ag NWs during plasmon propagation has been characterized recently.^{51,52}

Apart from the above very interesting optical properties of chemically synthesized silver NWs, we have demonstrated recently that branched NW structures can serve as routers and demultiplexers to control the direction of plasmon propagation in the branched structures, and further explained the mechanism

^aBeijing National Laboratory for Condensed Matter Physics and Institute of Physics, Chinese Academy of Sciences, Box 603-146, Beijing, 100190, China. E-mail: hxxu@iphy.ac.cn

^bDivision of Solid State Physics/The Nanometer Structure Consortium, Lund University, Box 118, Lund, S-221 00, Sweden

for such routing behavior theoretically.⁵³ Plasmon interference was used to modulate the plasmon propagation in Ag NW-based structures.⁵⁴ By using quantum dot fluorescence, we have imaged the electric field distributions around the NWs and found the dependence of the plasmon near field distribution on the incident polarizations and phases of the focused laser beams.⁵⁵ Based on SP interferences, a complete set of binary logic gates has been realized,⁵⁵ and these plasmonic logic gates have been even cascaded to realize more complex functions in simple NW networks.⁵⁶

In this work, we experimentally investigated SP interferences using a QD fluorescence imaging method in more detail, and revealed the principles to control SP interferences in silver NW networks. Silver nanowire structures composed of a main wire and a branch wire were used for the plasmon interference study. The two plasmon beams launched by an incident laser on the main wire terminal and the branch wire terminal interfere in the main NW and result in modulated emission intensity at the output terminal of the main NW. It is found that the near field distribution plays a central role in determining the strength of the plasmon interferences. When the excitation laser was focused on the terminal of the main wire, the near field distribution can be controlled by tuning the polarization of the incident light. When the antinode in the plasmon distribution pattern overlaps with the junction between the main wire and the branch wire, the two plasmon beams will interfere strongly because of the spatial overlap of the two plasmon beams at the junction. Contrarily, the plasmon interference is weak if the local-near field intensity is weak at the junction.

Experimental

The Ag nanowires are synthesized according to the reported protocol.⁵⁷ The as-prepared products are washed in ethanol through centrifugation for several times and redispersed in ethanol for future use. The ethanol containing Ag NWs are dropped onto clean glass slides and dried naturally. A micro-manipulator (MMO-202ND, Narishige) mounted on an upright optical microscope is used to manipulate individual NWs to make the branched structures. The mean radius of the NWs used in this work is about 150 nm. Then an Al₂O₃ layer of 30 nm thickness is deposited onto the sample using an atomic layer deposition machine (Cambridge NanoTech, Savannah-100) operating at 200 °C. Finally, quantum dots in water solution (Invitrogen, SKU# Q21321MP) are spin coated on top of the Al₂O₃ layer.

The optical measurements are based on an upright optical microscope (Olympus BX51). A HeNe laser operating at a wavelength of 633 nm was used for excitation of the propagating surface plasmons. The laser light is split into two beams and focused onto the ends of the main wire and the branch wire through a 100× objective (NA 0.95). The same objective is used for the signal collection. The polarization of the two laser beams can be controlled separately by rotating the half wave plates in the light paths. The phase difference between the two laser beams is controlled by tuning the Soleil-Babinet compensator in one of the light paths. The collected signal is recorded by a CCD camera (DVC-1412AM). To get the QD fluorescence, a long pass edge filter was used to block the excitation laser.

Results and discussion

Two plasmon beams can be launched from the main NW and the branch NW, and the two beams will interfere to modulate the intensity at the output terminal. For the structure shown in Fig. 1(a), the I1 and I2 terminals are used for plasmon excitation. Two laser beams were focused on the I1 and I2 terminals, respectively, to excite the propagating plasmons and resulted in the emission at the terminal O as shown in Fig. 1(b). The phase difference between the two laser beams was tuned by a compensator in the light path for I2 excitation. Fig. 1(c) and (d) show the output intensity oscillation as a function of the phase difference change for two different incident polarizations as indicated by the red arrows shown in the top-left corners of the panels. The polarization of the excitation light at the I2 terminal was kept fixed as in Fig. 1(b), which corresponds to the maximum output intensity when only I2 is illuminated. The green lines in Fig. 1(c) and (d) correspond to the output intensity at terminal O when either input beam is incident. We use visibility, defined as $(I_{\max} - I_{\min}) / (I_{\max} + I_{\min})$, to measure the strength of plasmon interference, where I_{\max} and I_{\min} are the maximum and minimum values of the output intensity. The interference curve in Fig. 1(c) has a visibility of larger than 0.8, while the curve in Fig. 1(d) has a visibility of less than 0.5. These results show that the plasmon interference is dependent on the polarization of the incident light at the main wire terminal.

As the NW structure is coated by QDs with an Al₂O₃ layer as the spacer, the QDs will be excited by the propagating plasmons and emit fluorescence.⁴⁵ The emission intensity of QDs is proportional to the local electromagnetic (EM) field intensity, thus the QDs can serve as local probes to report the local EM

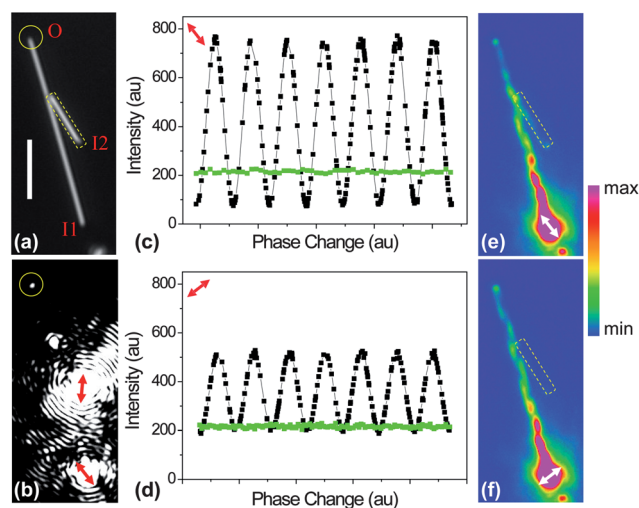


Fig. 1 (a) White light optical image of the NW structure. (b) The image for two laser beams focused on the two input terminals I1 and I2. (c and d) Black: the scattering intensity at terminal O as a function of the phase difference between the two laser beams corresponding to two different polarizations of the I1 input (red arrows). Green: scattering intensity at terminal O for either I1 or I2 input. (e and f) QD fluorescence images for I1 input of two different polarizations corresponding to (c) and (d), respectively. The scale bar in (a) is 5 μm. The red and white arrows indicate the polarization of the incident laser. The dashed rectangles outline the branch wire.

field intensity generated by the propagating plasmons. By detecting the QD fluorescence using the far field optical method, the near field distribution information can be obtained. From the QD fluorescence image in Fig. 1(e), it can be seen that the plasmon near field distribution is modulated showing a zigzag style pattern. This modulated near field distribution pattern is resulted from the superposition of different plasmon modes excited in the Ag nanowires.⁵⁸ As can be seen from Fig. 1(e), the junction between the main wire and the branch wire is overlapped with an antinode of the plasmon near field pattern. For the polarization shown in Fig. 1(f), the plasmon antinode is on the opposite side of the junction. Comparing Fig. 1(c)–(f), it can be speculated that the interference visibility is dependent on the near field distribution at the junction between the main NW and the branch NW. When the plasmon antinode is overlapped with the junction, the interference between the plasmon beams generated in the main wire and branch wire is stronger. If the plasmon antinode has no overlap with the junction, *i.e.* the local EM field intensity is very weak at the junction, the interference of the two plasmon beams is weak. This speculation is verified by our experimental data and will be discussed in detail in the later part of the paper. Since the plasmon near field distribution is dependent on the polarization of the excitation light, the interference visibility is dependent on the incident polarization at the main wire terminal.

For the NW structure shown in Fig. 2(a), i, the interference visibility was measured when the laser polarization at the main wire terminal was tuned in the range of 0 to 180 degrees. Fig. 2(a), ii–iv show the QD fluorescence images for different excitations. The excitation on the main wire terminal results in the near field distribution on the main wire determined by the incident polarization, as shown in Fig. 2(a), ii and iii. When the

laser was incident on the branch tip, plasmons were generated in the branch wire, which can be seen from the near field distribution pattern shown in Fig. 2(a), iv. Through the junction, the plasmons in the branch wire are transmitted to the bottom part of the main wire with a zigzag style near field distribution pattern. Fig. 2(b) shows the interference visibility dependence on the main wire incident polarization angle θ . The interference is strongest with I_{\max}/I_{\min} equal to 26, corresponding to the visibility of about 0.93 when θ is around 45°, and weakest with the visibility of about 0.28 when θ is around 125°. The QD fluorescence images in Fig. 2(a), ii and iii correspond to the polarizations for maximum and minimum interference visibility, respectively. For the incident polarization indicated in Fig. 2(a), ii, the plasmon antinode is distributed at the junction position, which results in a larger interference visibility. While for the polarization in Fig. 2(a), iii, the near field intensity at the junction is locally weak, which results in a smaller visibility. In Fig. 2(c), the scattering intensity at the output terminal O and the junction J with excitation only at the main wire end is plotted as a function of the polarization angle. The junction scattering intensity, which is dependent on the near field intensity at the junction, shows similar polarization dependence as the visibility.

The relationship between the plasmon antinode distribution and the interference visibility can be understood by considering the electromagnetic wave interference and the propagation of the plasmons in the nanowire. As we have discovered recently, the plasmons can propagate helically around the nanowire in a uniform medium if plasmon modes $m = \pm 1$ are excited equally and interfered with $m = 0$ mode.⁵⁸ The Ag nanowires studied here are placed on glass substrates and coated by an Al₂O₃ layer, so the nanowires are imbedded in an asymmetric medium. The interference of these modes results in the plasmon beating as evidenced by the zigzag type near field distribution pattern. For the plasmons excited from the main wire, the near field pattern can be controlled by tuning the polarization of the incident light. For the plasmons launched from the branch wire, they propagate to the junction and couple into the main wire. And the near field at the junction must be locally strong, no matter what the incident polarization is (in experiments, the polarization for I2 input is chosen as the polarization corresponding to the maximum output intensity for only the I2 input), to make the plasmon transmission to the main wire. For different polarizations of the input light at the branch wire terminal, the in-coupling efficiency of the plasmon transmission from the branch to the main wire is different. However, the plasmon modes excited in the main wire would be almost the same except for the intensity. So the near field distribution in the main wire for the branch excitation is insensitive to the incident polarization at the branch terminal, which makes the interference visibility less dependent on the branch input polarization. In experiments, the variation of the intensity was compensated by tuning the input power. Considering the interference of two electromagnetic waves, the emission intensity at the output terminal of the nanowire can be expressed as $|\vec{E}_m(\vec{r})|^2 + |\vec{E}_b(\vec{r})|^2 + 2|\vec{E}_m(\vec{r})||\vec{E}_b(\vec{r})|\cos(\Delta)$, where $E_m(r)$ and $E_b(r)$ are the electric fields of the plasmons excited from the main wire terminal and the branch wire terminal at position r around the output terminal, respectively, Δ is the phase difference between the two plasmon waves. The visibility is largest when the amplitudes of the electric field of the two plasmon waves $|\vec{E}_m(\vec{r})|$

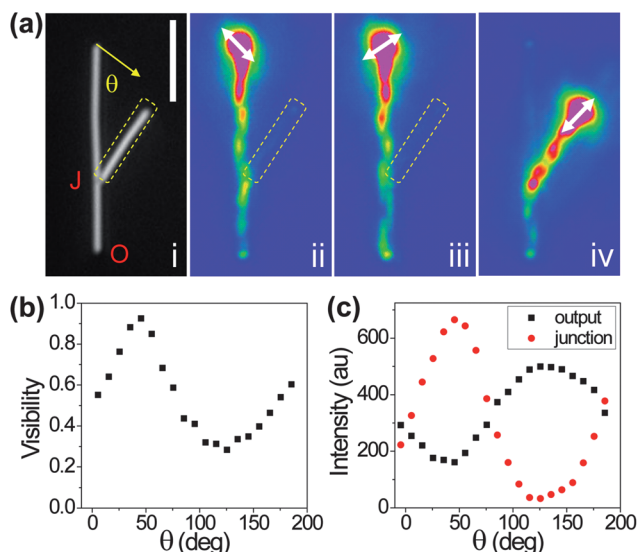


Fig. 2 (a) White light image (i) and QD fluorescence images for different excitations (ii) to (iv) of a branched NW structure. (b) The interference visibility as a function of the polarization angle of the laser beam incident on the main wire. (c) The scattering intensity at the output terminal O and the junction J as a function of the polarization angle of the laser beam incident on the main wire. The scale bar in (a) is 5 μm . The white arrows indicate the polarization of the incident laser. The dashed rectangles outline the branch wire.

and $|\vec{E}_b(\vec{r})|$ are the same. The near field generated by the branch excitation is strong at the junction, which determines the distribution of the near field on the main wire. For the plasmons excited at the main wire end, if the near field antinode is off the junction, the plasmons excited from the main wire end and from the branch wire end propagate along different routes on the wire, *i.e.* the amplitude difference of the electric field by main wire excitation and branch excitation is large at the same position, which determines that the interference of the two plasmon waves is quite incomplete resulting in the small visibility. Fig. 2(a), iv shows the near field distribution pattern when the plasmons are launched from the branch. Comparing the near field distribution on the main wire section below the junction in Fig. 2(a), iii and iv, the plasmon near field patterns distribute in an opposite way, which explains the very weak interference for that polarization. Depending on the detailed geometries of the structures, especially the junction, the interference visibility may be different for each individual structure. But for a given structure, the two plasmon beams interfere most strongly when the near field of the plasmons launched from the main wire is locally strong at the junction.

Although the detailed geometries of the nanowire ends and junctions can influence the exact behavior of the branched nanowire structures, extracting the fundamentals among the various factors is important and possible. Actually, the influences of the nanowire end facets and the distances between the nanowire terminals and the junctions can be reflected by the plasmon near field distributions. The shape of the main nanowire end will influence the in-coupling efficiency for light-plasmon conversion, and influence the relative intensity of the different modes excited in the main nanowire. The modulated near field intensity distribution is caused by the spatial beating of these plasmon modes. Therefore, the influence of the nanowire end geometries is included in the near field distribution pattern. Besides the nanowire end geometries, the polarization of the incident laser light also strongly influences the excitation of different plasmon modes and thus the near field pattern. By examining the near field pattern of the propagating plasmons, both the influences of the nanowire end structures and the incident polarizations are considered. As for the distances between the nanowire terminals and the junctions, the distances will mainly influence the number of nodes and antinodes over those distances and whether the junction can overlap completely with the antinode. Since the loss is inevitable during the plasmon propagation and the propagation lengths of different plasmon modes are different, after long distance propagation, the relative intensity of the different plasmon modes is changed and the contrast of the nodes and antinodes in the near field pattern may become unclear. The change of the near field pattern will influence the plasmon interference. Moreover, the near field pattern of plasmons is a more direct aspect to determine the plasmon interference. Since the longitudinal size of the plasmon antinode is between one micron and two microns, while the size of the junction is usually smaller than the NW diameter, *i.e.* tens to hundreds of nanometers, the position of the junction along the primary wire, which determines the degree of overlap for the plasmon antinode and the branch junction, should play an important role in the interference of the two plasmon beams. The detailed differences in the structures make their interference behavior show some differences.

The polarization dependence of the visibility shown in Fig. 2 is typical in all the measured data. However, a different behavior is also observed. For the structure shown in Fig. 3(a), i, when the laser on the main wire terminal polarized along the wire, the EM near field intensity was weak at the junction, *i.e.* the plasmon antinode was on the opposite side of the junction as shown in Fig. 3(a), ii. When the laser polarized perpendicular to the main wire, the plasmon antinode was on the junction as shown in Fig. 3(a), iii. The near field intensity at the junction does not seem strong in Fig. 3(a), iii, which is due to the bleaching of the QD fluorescence after long time laser illumination. Actually, the near field pattern difference of ii and iii can be clearly seen by comparing the section marked by the dashed rectangle along the main wire. The near field intensity pattern is distributed in an opposite way in Fig. 3(a), ii and iii. Therefore, the antinode in Fig. 3(a), iii is overlapped with the junction. Fig. 3(b) and (c) show the output intensity modulations caused by the two

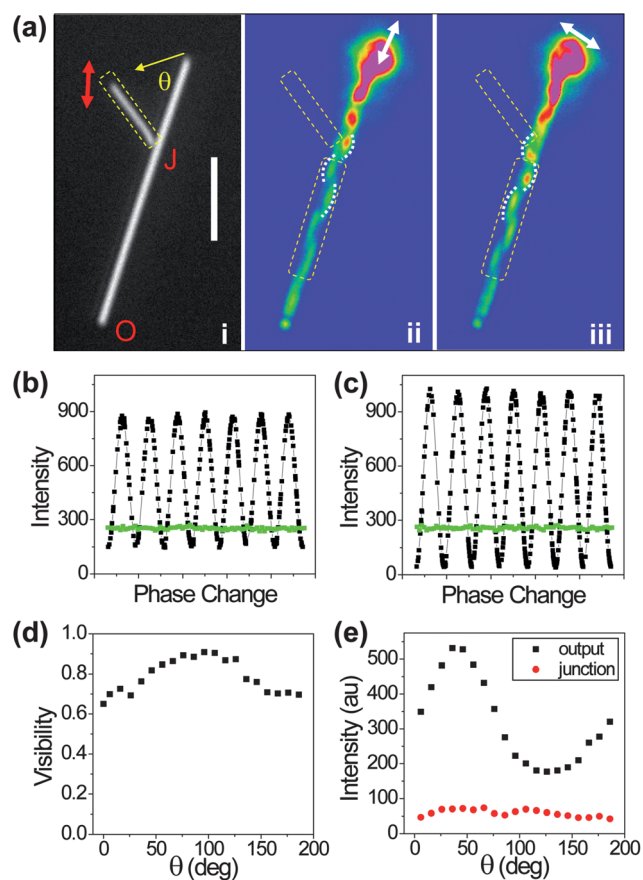


Fig. 3 (a) White light image (i) and QD fluorescence images for different excitations (ii) and (iii) of a branched NW structure. The scale bar is 5 μm . The white dotted curves in (ii) and (iii) are used to emphasize the outline of the near field antinodes. The red and white arrows indicate the polarization of the incident laser. (b and c) Black: the output intensity at terminal O as a function of the phase difference between the two laser beams, corresponding to the polarization in (ii) and (iii), respectively. Green: the scattering intensity at terminal O for either I1 or I2 input. (d) Interference visibility as a function of the polarization angle of the laser beam incident on the main wire. (e) Scattering intensity at the output end O and at the junction J as a function of the polarization angle of the laser beam incident on the main wire.

plasmon beam interferences corresponding to the polarization in Fig. 3(a), ii and iii, respectively. The interference visibility is smallest in Fig. 3(b), and largest in Fig. 3(c), which is consistent with the data shown in Fig. 1 and 2. From Fig. 3(d), it can be seen that the interference visibility dependence on the polarization angle is different from the structure in Fig. 2. The maximum value of the visibility is achieved when θ is about 90 degrees, and the minimum value appears when θ is about 0. The maximum visibility is larger than 0.9, and the minimum is about 0.67, which is still not a too weak interference. When only one laser beam is incident on the top end of the main wire, the scattering at the junction is weak for all polarizations (red dots in Fig. 3(e)), which probably means the connection between the main wire and the branch wire is so good that they almost behave like a unitary structure. This good connection may be one reason for the particular polarization dependence and relatively large minimum value of the visibility.

So far, only the polarization for the laser beam on the main wire terminal is changed to get different interference visibility. We further investigated the influence of the polarization of the input light at the branch end to the visibility. For the structure shown in Fig. 4(a), i, the QD images corresponding to the incident polarizations for maximum and minimum visibility are shown in Fig. 4(a), ii and iii. For the strongest interference, the visibility is about 0.72 (Fig. 4(b)). For the weakest interference, the minimum output intensity is still larger than the output intensity with one input laser beam, and the visibility is about 0.15 (Fig. 4(b)). In Fig. 4(b), the data of different polarizations for the laser beam on the branch wire terminal are also plotted.

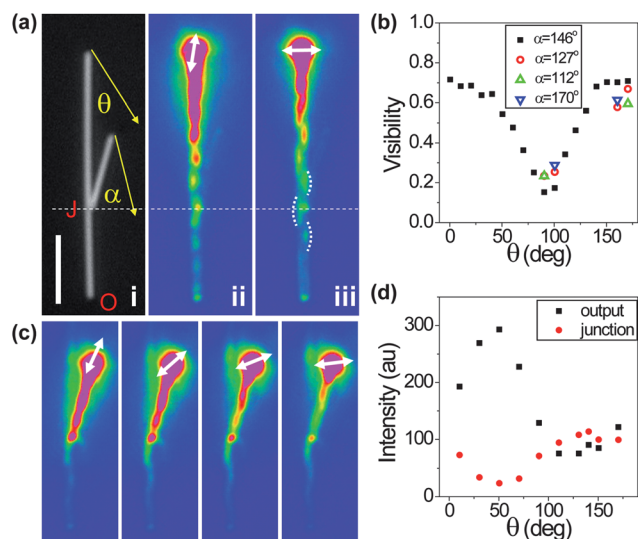


Fig. 4 (a) White light image (i) and QD fluorescence images for different excitations (ii) and (iii) of a branched NW structure. The white dotted curves in (iii) are used to emphasize the outline of the near field antinodes. The scale bar is 5 μm . (b) Interference visibility as a function of the polarization angle of the laser beam incident on the main wire. Symbols of different colors correspond to different polarizations of the laser beam at the branch terminal. (c) QD fluorescence images when excited at the branch terminal with different polarizations. (d) Scattering intensity at the output end O and at the junction J as a function of the polarization angle of the laser beam incident on the main wire. The white arrows indicate the polarization of the incident laser.

With the change of the polarization angle α , the interference visibility varies, but the variation is small compared with the variation as θ is changed. Fig. 4(c) shows the near field distribution images for excitation at the branch wire terminal with different polarizations. From those images, it can be seen that the near field distribution patterns on the main wire are quite similar for different polarizations of the laser beam on the branch terminal. This is because, whatever the incident polarization at the branch terminal is, the plasmon modes excited in the main wire section below the junction are mainly determined by the branch structure and the near field intensity at the junction is always locally strong. Fig. 4(d) shows the scattering intensity variations as a function of the polarization angle θ . The polarization dependence of the visibility also shows some similarity with the polarization dependence of the junction scattering intensity (red dots). The deviation of the θ values for the minimum visibility and the minimum scattering intensity at the junction may be caused by the different photon–plasmon conversion efficiency for input light of different polarizations and the specific near-field distribution determined by the structure geometries.

Conclusion

By launching two plasmon beams in branched nanowire structures, we experimentally investigated the plasmon interference which modulates the output intensity. It is found that the interference visibility is strongly dependent on the polarization of the incident laser light on the main wire terminal, but weakly dependent on the light polarization on the branch wire terminal. Using QD fluorescence to image the near field distribution induced by propagating plasmons, we found that the near field distribution plays a critical role in determining the plasmon interference. For the plasmons launched from the branch wire, the near field intensity at the junction is always locally strong to efficiently couple to the main wire, while for the plasmons launched from the main wire, the near field intensity at the junction is strongly dependent on the polarization of the excitation light. The strongest interference is obtained when the antinode in the near field pattern is overlapped with the junction between the main wire and the branch wire, because of the spatial overlap of the two plasmon beams. These results will be helpful for designing NW structures with strongly modulated output signals and controlling the plasmon propagation in metal NW networks.

Acknowledgements

This work was supported by MOST grant (no. 2009CB930700), NSFC grants (nos 10625418, 10874233, 11004237 and 11134013), “Knowledge Innovation Project” (KJJCX2-EW-W04) and Youth Innovation Promotion Association of CAS.

Notes and references

- 1 W. L. Barnes, A. Dereux and T. W. Ebbesen, *Nature*, 2003, **424**, 824–830.
- 2 M. Pelton, J. Aizpurua and G. Bryant, *Laser Photonics Rev.*, 2008, **2**, 136–159.
- 3 M. Schnell, A. Garcia-Etxarri, A. J. Huber, K. Crozier, J. Aizpurua and R. Hillenbrand, *Nat. Photonics*, 2009, **3**, 287–291.

- 4 J. A. Schuller, E. S. Barnard, W. S. Cai, Y. C. Jun, J. S. White and M. L. Brongersma, *Nat. Mater.*, 2010, **9**, 193–204.
- 5 H. A. Atwater and A. Polman, *Nat. Mater.*, 2010, **9**, 205–213.
- 6 H. X. Xu, E. J. Bjerneld, M. Kall and L. Borjesson, *Phys. Rev. Lett.*, 1999, **83**, 4357–4360.
- 7 H. X. Xu, J. Aizpurua, M. Kall and P. Apell, *Phys. Rev. E: Stat. Phys., Plasmas, Fluids, Relat. Interdiscip. Top.*, 2000, **62**, 4318–4324.
- 8 A. M. Michaels, J. Jiang and L. Brus, *J. Phys. Chem. B*, 2000, **104**, 11965–11971.
- 9 E. Prodan, C. Radloff, N. J. Halas and P. Nordlander, *Science*, 2003, **302**, 419–422.
- 10 H. Wei, U. Hakanson, Z. L. Yang, F. Hook and H. X. Xu, *Small*, 2008, **4**, 1296–1300.
- 11 H. Wei, F. Hao, Y. Z. Huang, W. Z. Wang, P. Nordlander and H. X. Xu, *Nano Lett.*, 2008, **8**, 2497–2502.
- 12 H. X. Xu, *Appl. Phys. Lett.*, 2004, **85**, 5980–5982.
- 13 K. Yoshida, T. Itoh, H. Tamaru, V. Biju, M. Ishikawa and Y. Ozaki, *Phys. Rev. B: Condens. Matter Mater. Phys.*, 2010, **81**, 115406.
- 14 M. L. Juan, M. Righini and R. Quidant, *Nat. Photonics*, 2011, **5**, 349–356.
- 15 L. M. Tong, V. D. Miljkovic, P. Johansson and M. Kall, *Nano Lett.*, 2011, **11**, 4505–4508.
- 16 Z. P. Li, M. Kall and H. Xu, *Phys. Rev. B: Condens. Matter Mater. Phys.*, 2008, **77**, 085412.
- 17 M. Righini, A. S. Zelenina, C. Girard and R. Quidant, *Nat. Phys.*, 2007, **3**, 477–480.
- 18 H. X. Xu and M. Kall, *Phys. Rev. Lett.*, 2002, **89**, 246802.
- 19 W. H. Zhang, L. N. Huang, C. Santschi and O. J. F. Martin, *Nano Lett.*, 2010, **10**, 1006–1011.
- 20 P. Muhlschlegel, H. J. Eisler, O. J. F. Martin, B. Hecht and D. W. Pohl, *Science*, 2005, **308**, 1607–1609.
- 21 S. Kim, J. H. Jin, Y. J. Kim, I. Y. Park, Y. Kim and S. W. Kim, *Nature*, 2008, **453**, 757–760.
- 22 K. M. Mayer and J. H. Hafner, *Chem. Rev.*, 2011, **111**, 3828–3857.
- 23 H. X. Xu and M. Kall, *Sens. Actuators, B*, 2002, **87**, 244–249.
- 24 H. Wei, A. Reyes-Coronado, P. Nordlander, J. Aizpurua and H. X. Xu, *ACS Nano*, 2010, **4**, 2649–2654.
- 25 E. Ozbay, *Science*, 2006, **311**, 189–193.
- 26 S. A. Maier, P. G. Kik, H. A. Atwater, S. Meltzer, E. Harel, B. E. Koel and A. A. G. Requicha, *Nat. Mater.*, 2003, **2**, 229–232.
- 27 B. Lamprecht, J. R. Krenn, G. Schider, H. Ditlbacher, M. Salerno, N. Felidj, A. Leitner, F. R. Aussenegg and J. C. Weeber, *Appl. Phys. Lett.*, 2001, **79**, 51–53.
- 28 D. F. P. Pile and D. K. Gramotnev, *Opt. Lett.*, 2004, **29**, 1069–1071.
- 29 S. I. Bozhevolnyi, V. S. Volkov, E. Devaux, J. Y. Laluet and T. W. Ebbesen, *Nature*, 2006, **440**, 508–511.
- 30 I. De Leon and P. Berini, *Nat. Photonics*, 2010, **4**, 382–387.
- 31 A. Manjavacas and F. J. G. de Abajo, *Nano Lett.*, 2009, **9**, 1285–1289.
- 32 X. W. Chen, V. Sandoghdar and M. Agio, *Nano Lett.*, 2009, **9**, 3756–3761.
- 33 L. Cao, R. A. Nome, J. M. Montgomery, S. K. Gray and N. F. Scherer, *Nano Lett.*, 2010, **10**, 3389–3394.
- 34 E. J. Smith, Z. W. Liu, Y. F. Mei and O. G. Schmidt, *Nano Lett.*, 2010, **10**, 1–5.
- 35 H. Ditlbacher, A. Hohenau, D. Wagner, U. Kreibig, M. Rogers, F. Hofer, F. R. Aussenegg and J. R. Krenn, *Phys. Rev. Lett.*, 2005, **95**, 257403.
- 36 Z. P. Li, F. Hao, Y. Z. Huang, Y. R. Fang, P. Nordlander and H. X. Xu, *Nano Lett.*, 2009, **9**, 4383–4386.
- 37 T. Shegai, V. D. Miljkovic, K. Bao, H. X. Xu, P. Nordlander, P. Johansson and M. Kall, *Nano Lett.*, 2011, **11**, 706–711.
- 38 Z. P. Li, K. Bao, Y. R. Fang, Y. Z. Huang, P. Nordlander and H. X. Xu, *Nano Lett.*, 2010, **10**, 1831–1835.
- 39 M. Allione, V. V. Temnov, Y. Fedutik, U. Woggon and M. V. Artemyev, *Nano Lett.*, 2008, **8**, 31–35.
- 40 C. Rewitz, T. Keitzl, P. Tuchscherer, J. Huang, P. Geisler, G. Razinskas, B. Hecht and T. Brixner, *Nano Lett.*, 2012, **12**, 45.
- 41 Y. Fedutik, V. V. Temnov, O. Schops, U. Woggon and M. V. Artemyev, *Phys. Rev. Lett.*, 2007, **99**, 136802.
- 42 Y. Fedutik, V. Temnov, U. Woggon, E. Ustinovich and M. Artemyev, *J. Am. Chem. Soc.*, 2007, **129**, 14939–14945.
- 43 A. V. Akimov, A. Mukherjee, C. L. Yu, D. E. Chang, A. S. Zibrov, P. R. Hemmer, H. Park and M. D. Lukin, *Nature*, 2007, **450**, 402–406.
- 44 R. Kolesov, B. Grotz, G. Balasubramanian, R. J. Stohr, A. A. L. Nicolet, P. R. Hemmer, F. Jelezko and J. Wrachtrup, *Nat. Phys.*, 2009, **5**, 470–474.
- 45 H. Wei, D. Ratchford, X. Q. Li, H. X. Xu and C. K. Shih, *Nano Lett.*, 2009, **9**, 4168–4171.
- 46 S. D. Liu, M. T. Cheng, Z. J. Yang and Q. Q. Wang, *Opt. Lett.*, 2008, **33**, 851–853.
- 47 M. Frimmer, Y. T. Chen and A. F. Koenderink, *Phys. Rev. Lett.*, 2011, **107**, 123602.
- 48 X. Guo, M. Qiu, J. M. Bao, B. J. Wiley, Q. Yang, X. N. Zhang, Y. G. Ma, H. K. Yu and L. M. Tong, *Nano Lett.*, 2009, **9**, 4515–4519.
- 49 R. X. Yan, P. Pausauskie, J. X. Huang and P. D. Yang, *Proc. Natl. Acad. Sci. U. S. A.*, 2009, **106**, 21045–21050.
- 50 Y. R. Fang, H. Wei, F. Hao, P. Nordlander and H. X. Xu, *Nano Lett.*, 2009, **9**, 2049–2053.
- 51 Z. P. Li, K. Bao, Y. R. Fang, Z. Q. Guan, N. J. Halas, P. Nordlander and H. X. Xu, *Phys. Rev. B: Condens. Matter Mater. Phys.*, 2010, **82**, 241402.
- 52 W. H. Wang, Q. Yang, F. R. Fan, H. X. Xu and Z. L. Wang, *Nano Lett.*, 2011, **11**, 1603–1608.
- 53 Y. R. Fang, Z. P. Li, Y. Z. Huang, S. P. Zhang, P. Nordlander, N. J. Halas and H. X. Xu, *Nano Lett.*, 2010, **10**, 1950–1954.
- 54 Z. P. Li, S. P. Zhang, N. J. Halas, P. Nordlander and H. X. Xu, *Small*, 2011, **7**, 593–596.
- 55 H. Wei, Z. P. Li, X. R. Tian, Z. X. Wang, F. Z. Cong, N. Liu, S. P. Zhang, P. Nordlander, N. J. Halas and H. X. Xu, *Nano Lett.*, 2011, **11**, 471–475.
- 56 H. Wei, Z. X. Wang, X. R. Tian, M. Kall and H. X. Xu, *Nat. Commun.*, 2011, **2**, 387.
- 57 Y. G. Sun and Y. N. Xia, *Adv. Mater.*, 2002, **14**, 833–837.
- 58 S. P. Zhang, H. Wei, K. Bao, U. Hakanson, N. J. Halas, P. Nordlander and H. X. Xu, *Phys. Rev. Lett.*, 2011, **107**, 096801.